Available online at www.sciencedirect.com
ScienceDirect
Journal of Bionic Engineering 9 (2012) 156–165

A Novel Implementation of a Flexible Robotic Fin Actuated by Shape Memory Alloy

Qin Yan[1,2], Lei Wang[1], Bo Liu[1], Jie Yang[1], Shiwu Zhang[1]

1. *Department of Precision Machinery and Precision Instrumentation*, *University of Science and Technology of China*, *Hefei* 230026, *P. R. China*
2. *Department of Mechanical and Electrical Engineering*, *Suzhou University of Science and Technology*, *Suzhou* 215011, *P. R. China*

Abstract

In this paper, study of a novel flexible robotic-fin actuated by Shape Memory Alloy (SMA) is presented. The developed robotic fin is capable of implementing various 3-Dimensional (3D) motions, which plays an important role in robot propulsion and maneuverability. Firstly, the morphological and mechanics parameters of a real pectoral fin from a carp are investigated. Secondly, a detailed design of the flexible pectoral fin driven by SMA is presented according to the previous morphological and mechanics analyses. Thirdly, a simplified theoretical model on the SMA fin plate is derived. The thermodynamics of the SMA plate and the relationship between curvature and phase transformation are analyzed. Finally, several simulations and model experiments are conducted according to the previous analyses. The results of the experiments are useful for the control of the robotic fin. The experimental results reveal that the SMA actuated fin ray has a good actuating performance.

Keywords: shape memory alloy, robotic fin, SMA fin plate

doi: 10.1016/S1672-6529(11)60111-X

1 Introduction

Fish exhibit various marvelous swimming abilities under water. They employ the bodies and/or fins to produce propulsive and maneuvering force. Fish swimming modes can be classified into two categories: Body and/or Caudal Fin (BCF) and Median and/or Paired Fin (MPF)[1].

Recent research revealed that fish fin plays an important role in fish swimming. In particularly, the pectoral fin is crucial in fish maneuvers such as hovering, turning, accelerating and braking[2,3]. With the development of Underwater Unmanned Vehicle (UUV), various forms of robotic fish fins have been developed[4–6], and the kinematics analysis, Computational Fluid Dynamics (CFD) of fin hydrodynamics, propulsive mechanism and experimental hydrodynamics of fins have been reported.

Lauder's group[7,8] paid great attention on the propulsive mechanism of fins, especially pectoral fin. They carried out a series of researches on kinematics, experimental hydrodynamics and CFD analysis of bluegill sunfish fin. The work discovered that pectoral fin can provide considerable lift, span-wise and thrust forces during sunfish cruising and turning movement[9]. The team also developed a flexible robotic pectoral fin actuated by servomotors[10], but the robotic fin actuated by servomotors is too bulky to be employed in a robotic fish. Low's group[11–13] developed a modular stingray propelled by pectoral fins to investigate the undulation mechanism of MPF fish. To examine the agility and the maneuverability of UUV, Toda's group developed a fish-like underwater vehicle with two undulating side fins composed of rigid fin rays driven by servomotor[14,15]. Hu *et al.* carried out a study of kinematics, CFD simulation and model experiment on the single long fin of Gymnarchus niloticus[16]. Wang *et al.* developed a SMA driven robot squid, which is capable of cruising and turning in the water[17,18]. We also conducted an experimental investigation on propulsive performance of a carangiform robotic fish[19] and CFD simulations on 2D undulatory mechanical fins actuated by SMA[20,21].

Corresponding author: Shiwu Zhang
E-mail: swzhang@ustc.edu.cn

To summarize, a great effort has been devoted to developing robotic fins. However, two outstanding features are important for a robotic fin according to the morphological and hydrodynamics study of a real fin: (1) the robotic fin should be flexible so that it can provide a positive propulsion during the whole movement cycle as a fish fin does[22,23]; (2) the robotic fin possesses a complex morphology that is similar to a fish fin, so that it can switch within different gestures to propel and maneuver efficiently. Based on the above consideration, we develop a novel flexible robotic fin actuated by SMA. The developed robotic fin can exhibit five fundamental gestures, and switch them to provide propulsion and maneuver force as a pectoral fin. The SMA actuated fin is also simple and easy to control, so that it is convenient to be equipped in a robotic fish.

The remainder of the paper is organized as follows. Section **2** introduces the morphological and mechanics study on the pectoral fins of a carp. Section **3** provides a detailed design of a robotic pectoral fin actuated by SMA. Section **4** presents a theoretical analysis of an SMA driven fin ray which is the basis to the control of the robotic fin. Section **5** discusses a set of simulation-based experiments. Section **6** describes several model experiments which verify the design and simulation results of the robotic fin. Section **7** concludes the paper by summarizing the important features of the robotic fish fin.

2 Morphologic and mechanics characteristics of a pectoral fin

Carp is a kind of typical carangiform fish, which has a highly effective and highly maneuverable swimming ability with the help of its pectoral fins. Therefore, we take carp as our example to measure the morphological parameters of the pectoral fin, as shown in Table 1 and Fig. 1.

Furthermore, the kinematic pattern of the pectoral fins was investigated with a high resolution digital camera (CASIO EX-F1). The captured pictures reveal that the pectoral fins are highly flexible as to display many complex 3D motions. Fig. 2 displays the action of the pectoral fins when the carp turns and retreats. Fig. 2a shows a snap shot of the pectoral fin as the carp turns, in the course of which the left pectoral fin (white arrows side) first expands, then strikes slowly against the body, while the right pectoral fin (black arrows side) first expands, then strikes away from the body. Fig. 2b shows a snap shot of the pectoral fin as the carp retreats, in the course of which both pectoral fins first expand perpendicularly to the fish body axis, then flap back and forth with a certain frequency.

Table 1 Morphological parameters of a carp pectoral fin

Morphological parameters	Value
The body length of the carp (mm)	210
The area of the pectoral fin (mm^2)	700
The number of fin rays belong to the fin	15
The length of the longest fin ray (mm)	37
The length of the shortest fin ray (mm)	16

(a) A carp pectoral fin

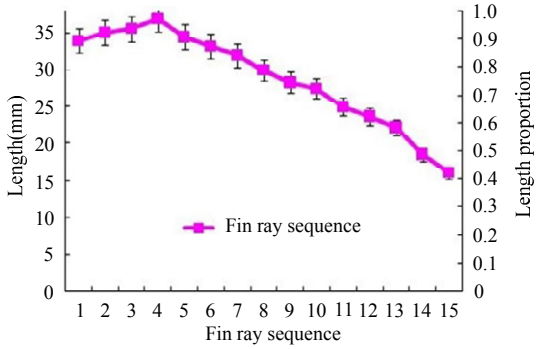

(b) The length of fin rays

Fig. 1 Morphological parameters of a carp pectoral fin. The grid is 5 mm × 5 mm in (a). In (b), the left *y*-axis denotes the length of each fin ray, while the right *y*-axis denotes the ratio of the length of each fin ray to the longest one.

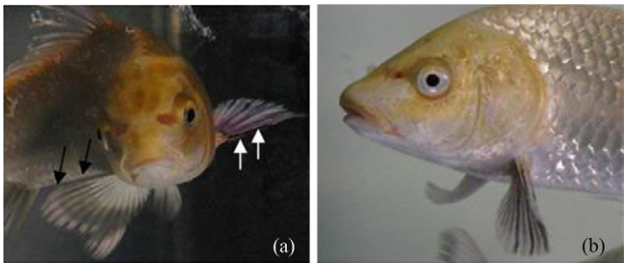

Fig. 2 Pectoral fins of carp in maneuverability. (a) Turning; (b) retreating.

The movements of the pectoral fins are so complex, which are difficult to reproduce by artificial pectoral fins. Fortunately, from plentiful images of the pectoral fins when a carp performs maneuvers such as cruising, turning, braking, retreating, descending and ascending, some basic gestures are found, which are relaxation, expansion, bending, cupping and undulation, as shown in Fig. 3. Lauder's group[7,8] also observed the same patterns of sunfish swimming.

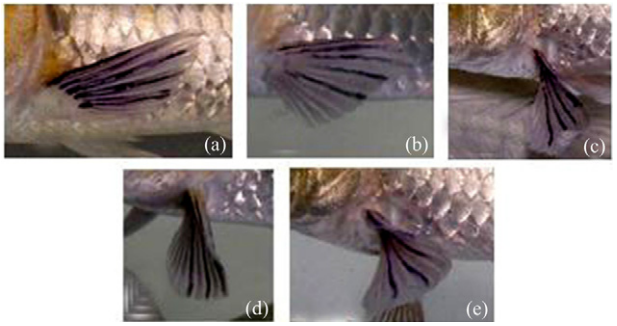

Fig. 3 Five basic gestures of the pectoral fin. (a) Relaxation; (b) expansion; (c) bending; (d) cupping; (e) undulation.

The mechanical properties of a fin ray are significant for developing a robotic fin. In order to obtain the distribution of bending stiffness and Young's modulus of the pectoral fin ray, we adopt a three-point bending-measurement approach in the experiment, as shown in Fig. 4. From the base side to the distal side, five fin rays (Fin ray No. 1, 3, 5, 7, and 9) are respectively selected for testing. For each fin ray, two locations are detected: 30% and 50% length of the fin ray. By pressing the dynamometer, the force on the fin ray changes and the deformation of the fin ray is displayed by the dial indicator, thus the bending stiffness is calculated. The stiffness of one location is calculated for five times with changing force, and the standard deviations are also obtained. The experimental results are shown in Figs. 5 and 6.

It can be seen from Figs. 5 and 6 that both bending stiffness and Young's modulus decrease from Fin Ray 1 to Fin Ray 9. As for each fin ray, Young's modulus of 30% length location is nearly 1.1 times as that of 50% length location.

In our research, Ni-Ti SMA plates are employed as the fin rays for robotic pectoral fin. Both bending stiffness and Young's modulus of SMA plates are approximate to that of the carp's fin rays, which are shown in Figs. 5 and 6. In these figures, K_M and E_M denote respectively bending stiffness and Young's modulus of SMA plates in martensite phase. However, E_A denotes Young's modulus of SMA plates in austenite phase, which means that SMA plates are stiffer when they actuate.

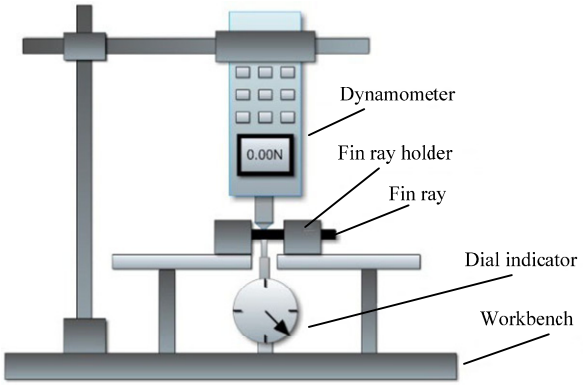

Fig. 4 Equipment for testing mechanical properties of fin rays.

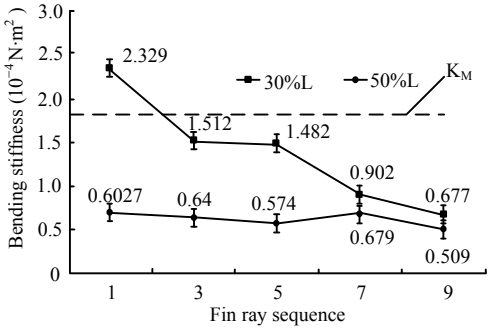

Fig. 5 Bending stiffness of the respective fin rays. The standard deviations are in the range of (0.002 to 0.031)×10^{-4} N·m^{-2}.

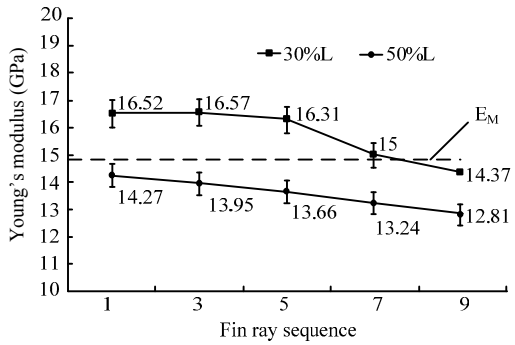

Fig. 6 Young's modulus of the respective fin rays. The standard deviations are in the range of (0.04 to 0.257) GPa. E_M = 14.8 GPa, E_A = 39.3 GPa.

3 Design of the robotic fin

3.1 Mechanical structure

SMA is adopted as the actuator of the robotic fin for the following advantages: (1) simplification; (2) larger-strain and larger stress; and (3) long life cycling, which

is up to 1×10^6 times. Considering the simplicity and easy controlling, the number of the fin rays is reduced to five, which enables the robotic fin to accomplish at least one cycle in its undulation. The mechanical structure of the robotic fin is shown in Fig. 7. The pectoral robotic fin mainly consists of three parts: fin base, fin rays, and flexible membrane.

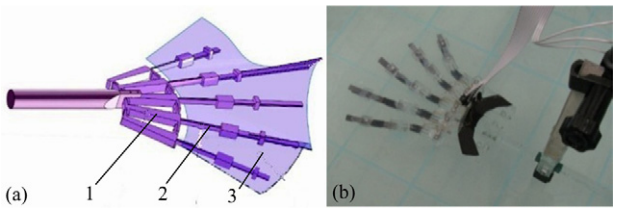

Fig. 7 Structure of a robotic pectoral fin. (a) The mechanical design of the robotic pectoral fin. 1 Fin base, 2 Fin rays, 3 Flexible membrane; (b) the robotic fin under water.

The basic unit of the fin ray is SMA plate. As shown in Fig. 8, two parallel SMA plates compose an SMA couple. An SMA couple can perform a bi-directional bending action when two SMA plates are heated alternatively. Each SMA fin ray contains two SMA couples which are assembled serially with orthogonal cross sections. Therefore, the SMA fin ray can bend in two orthogonal directions. Instead of heating SMA directly by electric current, we adopt the "enwinding heating" method to actuate an SMA plate. We wind the enamel-insulated copper wire closely over the SMA plate, then cover the copper wire with a PVC tube to protect them from water. Consequently, a low current passing through the copper wire is able to heat SMA plate quickly. Also, the SMA plate can cool down quickly under water. The latter experimental results prove that the actuating method is effective.

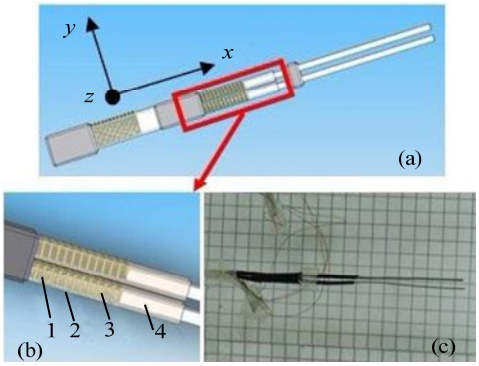

Fig. 8 Structure of a fin ray. (a) SMA fin ray; (b) SMA couple, 1 enamel-insulated copper wire, 2 PVC tube, 3 SMA with shape memory effect, 4 SMA without shape memory effect; (c) SMA couple under water.

Fin base also consists of two parallel SMA plates, which can perform a bi-directional bending action. Therefore, the SMA pectoral fin can maintain free and bending states. The elastic membrane, made of thin rubber, is adhered to the fin rays. It can elongate more than 150% of its initial length to fulfil a large deformation in various motions of the robotic fin.

According to the above morphological study, the complex motions of a real pectoral fin mainly include five basic gestures: relaxation, expansion, bending, cupping and undulation. During cruising and maneuvering, a fish frequently shifts these gestures of pectoral fins to balance, to position and to propel itself. Correspondingly, the five basic gestures of the robotic fin are well achieved by the coordinating control of the fin base and fin rays, as shown in Fig. 9.

3.2 Actuation mechanism

Fig. 10 displays the actuation mechanism of an SMA couple. In the figure, states 1, 2 and 3 represent up-bending state, relaxed state and down-bending state respectively. When heated to the austenite transformation temperature, A_s, SMA plate A bends up to bring the SMA couple to up-bending state. When SMA plate A cools, the SMA couple will recover to relaxed state. When heated to A_s, SMA plate B bends down and bring the SMA couple to down-bending state.

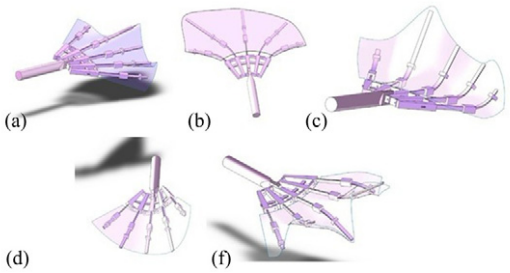

Fig. 9 Basic gestures of a robotic pectoral fin. (a) relaxation; (b) expansion; (c) bending; (d) cupping; (e) undulation.

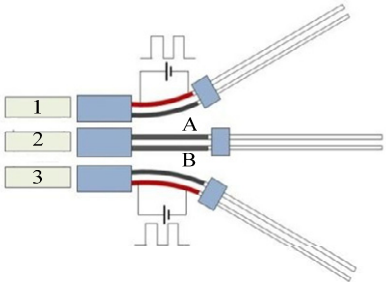

Fig. 10 Actuating principle of the plate mode. 1 Up-bending state, 2 Relaxed state, 3 Down-bending state.

4 Theoretical analysis of the SMA plate

4.1 Thermodynamics of SMA plate

Usually, SMA wires are heated by electric current. However, the SMA plate has a bigger volume, and needs more energy than SMA wires. As a result, it is inappropriate to heat the SMA plate directly with electric current. Alternatively, we adopt a novel heating method called "enwinding heating", as described in section **3**.

Three assumptions are made in the thermodynamic analysis of SMA plate: (1) The PVC tube is thin. It covers the enamel-insulated copper wire and the SMA plate closely and tightly. The tube, copper wire and SMA plate can be considered as an integrated plate. (2) Radiation can be ignored because of little amount of radiation of the tube, copper wire and SMA plate. (3) The convection between the integrated plate and water is presumed as the only way to transfer heat from the plate to environment.

When the SMA plate is heated, the energy balance is expressed as

$$E_i = E_{\text{sma}} + E_{\text{pvc}} + E_{\text{wire}} + E_{\text{con}} + E_{\text{ph}}, \tag{1}$$

$$E_i = i^2 \lambda_{\text{wire}} \frac{l_{\text{wire}} d_{\text{wire}}^2}{4\pi} t, \tag{2}$$

$$E_{\text{sma}} = \int_{T_s}^{T_f} c_{\text{sma}} \rho_{\text{sma}} l_{\text{sma}} \mathrm{d}w\mathrm{d}T(t), \tag{3}$$

$$E_{\text{pvc}} = \int_{T_s}^{T_{f1}} c_{\text{pvc}} \rho_{\text{pvc}} l_{\text{pvc}} \mathrm{d}w\mathrm{d}T(t), \tag{4}$$

$$E_{\text{wire}} = \int_{T_s}^{T_{f2}} c_{\text{wire}} \rho_{\text{wire}} l_{\text{wire}} \frac{\pi d_{\text{wire}}^2}{4} \mathrm{d}T(t), \tag{5}$$

$$E_{\text{con}} = \int_{t_s}^{t_f} h_w l_{\text{con}} 2(d+w)(T_f - T_s)\mathrm{d}t, \tag{6}$$

where E_i, E_{sma}, E_{pvc}, E_{wire}, E_{con}, and E_{ph} denote electric energy, the heat change of SMA, the heat change of PVC tube, the heat change of copper wire, convection energy between plate and water, and transformation latent heat of SMA, respectively; i denotes heating current through copper wire; λ_{wire} denotes electric resistivity of the copper wire; c_{wire}, c_{sma} and c_{pvc} denote the thermal capacities of copper wire, SMA plate and PVC tube, respectively; ρ_{wire}, ρ_{sma} and ρ_{pvc} denote the densities of copper wire, SMA plate and PVC tube, respectively; l_{wire}, l_{sma} and l_{pvc} denote the effective lengths of copper wire, SMA plate and PVC tube, respectively; d and w denote the depth and width of the SMA plate, respectively; T_s denotes the environment temperature; T_f, T_{f1} and T_{f2} denote the final temperatures of SMA plate, PVC tube and enamel-insulated copper wire respectively during the martensite reverse transformation process. t_s and t_f denote the start moment and finish moment of the heating process, respectively; h_w denotes the equivalent convective heat transfer coefficient.

The cooling process of SMA plate is a natural convective phenomenon. The energy exchange during the cooling process is given by

$$0 = E_{\text{sma}} + E_{\text{pvc}} + E_{\text{wire}} + E_{\text{con}} + E_{\text{ph}}, \tag{7}$$

$$E_{\text{sma}} = \int_{T_s}^{T_f} c_{\text{sma}} \rho_{\text{sma}} l_{\text{sma}} \mathrm{d}w\mathrm{d}T(t), \tag{8}$$

$$E_{\text{wire}} = \int_{T_s}^{T_{f2}} c_{\text{wire}} \rho_{\text{wire}} l_{\text{wire}} \frac{\pi d_{\text{wire}}^2}{4} \mathrm{d}T(t), \tag{9}$$

$$E_{\text{pvc}} = \int_{T_s}^{T_{f1}} c_{\text{pvc}} \rho_{\text{pvc}} l_{\text{pvc}} \mathrm{d}w\mathrm{d}T(t), \tag{10}$$

$$E_{\text{con}} = \int_{t_s}^{t_f} h_w l_{\text{con}} 2(d+w)(T_f - T_s)\mathrm{d}t. \tag{11}$$

For the sake of convenience, we consider h_w as a constant in both heating and cooling processes. From Eq. (1) to Eq. (11), the energy exchange can be estimated in both heating and cooling processes. However, it is difficult to obtain an accurate result through an analytic calculation, so we conduct a simulation to obtain the actuation time of the SMA plate in both heating and cooling processes.

4.2 Relationship between curvature and phase transformation of SMA plates

Many constitutive equations of SMA have been put forward to describe the mechanical and thermodynamical characteristics of SMA, including Tanaka's model[24], the first constitutive model of SMA, and Liang's[25] and Brinson's[26] models, both of which are revised versions of Tanaka's model. However, these models describe the stretching motion of SMA wires, not the bending motion of SMA plates. Therefore, we adopt a simplified model to describe the bending motion of

SMA plates, with regard to which some basic facts are taken into consideration. Firstly, SMA plates are very light and the actuation frequency of SMA plates is relatively low (about 1 Hz), so the inertia force can be neglected. Secondly, considering the constitutive model of SMA plates is absent, we take the curvature of SMA plates as the characteristic parameter of the bending motion. The relationship between the curvature and the phase transformation of SMA plates is described as[27]

$$k_{\mathrm{SMA}} = (1-\xi)k_{\max}, \tag{12}$$

where ξ denotes the martensite volume fraction which represents the degree of the martensite phase transformation. $k_{\max}$ denotes the trained maximum curvature, while k_{SMA} denotes the curvature in phase transformation. When ξ equals to 1, the phase transformation has not yet started, and the curvature is zero, while ξ equals to 0, the phase transformation has finished, and the curvature has reached the predefined one. ξ is defined as

$$\xi(T) = \frac{\xi_a}{1+e^{\alpha(T-T_0)}} + \xi_b. \tag{13}$$

In the cooling process of SMA, the parameters of Eq. (13) are

$$T_0 = \frac{M_s + M_f}{2}, \tag{14}$$

$$\alpha = \frac{\beta}{M_s - M_f}. \tag{15}$$

In the heating process of SMA, the parameters of Eq. (13) are:

$$T_0 = \frac{A_s + A_f}{2}, \tag{16}$$

$$\alpha = \frac{\beta}{A_f - A_s}. \tag{17}$$

in Eqs. (14) – (17), M_s, M_f, denote the starting and finishing temperatures of martensite phase transformation; A_s, A_f the starting and finishing temperatures of austenite phase transformation, respectively; β is determined empirically. In Eq. (13), ξ_a and ξ_b are constants.

5 Simulation experiments on SMA fin plate

In this section, we present two simulation experiments on SMA fin plate based on the analysis in section **4**. First, the temperature of the SMA plate with a heating current is investigated by simulation. Then, with the simulation results and Eqs. (12) – (17), the relationship between the curvature of SMA plate and time can be obtained.

5.1 Thermodynamic simulation

The thermodynamics of SMA plate is numerically computed with ANSYS. The effect of the the input current is studied. The equivalent convective heat transfer coefficient h_w can be obtained from aquarium experiments, and the experimental results indicate that h_w lies in the range of 800 w·m^{-2}·K^{-1} to 3000 w·m^{-2}·K^{-1} according to the thickness of PVC tube. In our simulation, h_w is set as 2000 w·m^{-2}·K^{-1}. The transformation temperature of NiTi SMA plates are M_f = 34.1˚C, M_s = 42.3˚C, A_s = 45.2˚C, A_f = 54.8˚C. The transformation latent heat of the SMA is measured with Differential Scanning Calorimetry (DSC), which is 9.101×10^3 J·kg^{-1}, (59.52×10^6 J·m^{-3} in enthalpy form). It is drawn from Fig. 11 that the enthalpy change is linear in the transformation process (T: 45.2˚C – 54.8˚C). The physical and mechanical properties of enamel-insulated copper wire, SMA plate and PVC tube are listed in Table 2.

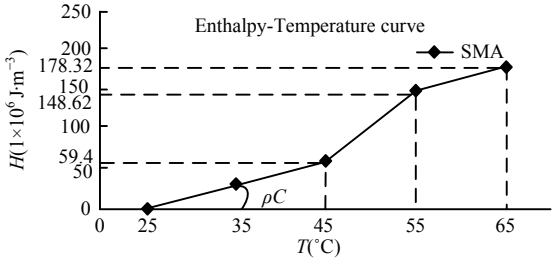

Fig. 11 Enthalpy of SMA as a function of temperature.

Table 2 Properties of copper wire, SMA plate and PVC tube, where ρ, C, λ, k and h_w represent density, thermal capacity, electric resistivity, thermal conductivity and convective heat transfer coefficient, respectively.

Parameters	Values		
	SMA plate	Copper wire	PVC tube
Dimension (mm)	Length: 100; Width: 4; depth: 0.5	Length: 100; Diameter: 0.1	Thickness: 0.1
ρ (kg·m^{-3})	6450	7900	1380
C (J·kg^{-1}·K^{-1})	460	390	900
λ (Ωm)	8.1×10^{-7}	1.85×10^{-8}	Insulator
k (w·m^{-1}·K^{-1})	10	401	0.16
h_w (w·m^{-2}·K^{-1})		800 – 3000	

To investigate the actuation speed of SMA plate, we conduct seven simulations with the current changing

from 0.8 A to 3.5 A, in which $h_w = 2000$ w·m^{-2}·K^{-1}. The simulation results are shown in Fig. 12, in which I is the current. The curves can be classified into two categories. In the cases with the currents of 0.8 A and 1 A, the SMA temperature can not reach A_f, because of the low heat flux. For the cases with the currents ranging from 1.5 A to 3.5 A, the SMA temperature can reach A_f, and the actuation time for temperature reaching A_f (heating time) becomes shorter with the increase in the current. The minimum heating time occurs in the case with the currents of 3.5 A, which is only 0.15 s. For each curve of the currents from 1.5 A to 3.5 A, the changing rate of the temperature has an obvious decline within the interval [45.2˚C, 54.8˚C], which is the effect of transformation latent heat of SMA plate. The cooling time is about 0.6 s for all the cases.

From Fig. 12, we can conclude that the actuation speed of the SMA plate increases as the current rises. It also indicates that the current should be set from 2 A to 3 A, where the actuating speed of SMA plate is fast enough.

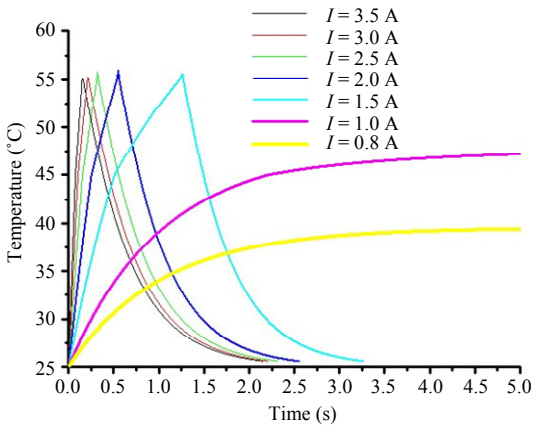

Fig. 12 Temperature of the SMA plate as a function of time for different currents. When the currents are 0.8 A and 1 A, the balance temperature are 38˚C and 46˚C respectively, and when the currents are 1.5 A, 2 A, 2.5 A, 3 A and 3.5 A, the actuation time are about 1.24 s, 0.54 s, 0.32 s, 0.21 s and 0.15 s, respectively.

5.2 Angular displacement of SMA fin plate

According to the analysis in section **4**, the curvature of SMA plate is determined by the martensite volume fraction which is in turn determined by the temperature of SMA plate. Combining the thermodynamics simulation results and Eqs. (12) – (17), we obtain the curvature change with heating time with respect to various currents. We substitute the curvature with angular displacement in correspondence to the model experiments in section **6**, since the latter is easier to measure in the actual experiments. The simulation is conducted with Matlab, and the result is displayed in Fig. 13. The results can be classified into two categories: (1) For the cases with the current of 0.8 A and 1 A, the temperature of SMA can not reach A_f, so the phase transformation is not fully completed, son the angular displacement can not reach the trained value; (2) For the cases of other currents, the phase transformation is fully completed, and the angular displacement reaches 118˚, which is the trained angular displacement. However, different currents lead to different response times. Furthermore, we can see that it only takes 0.15 s to finish the bending motion and reach the trained angular displacement when I equals 3.5 A, while it takes 1.24 s when I equals 1.5 A.

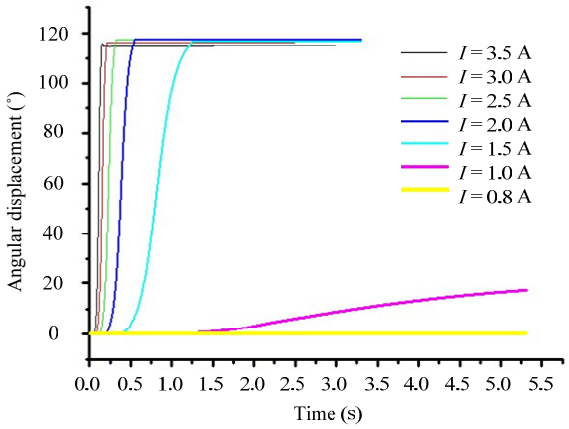

Fig. 13 Angular displacement of SMA plate with respect to currents.

6 Actuation experiments of SMA fin plates

To investigate the performance of SMA fin plates, we conducted a series of underwater actuation experiments of SMA plates. The properties of the SMA plates are the same as the ones in the simulations as listed in Table 2. The actuation speed, the maximum displacement and the torque output of SMA plates are the key factors observed in the experiments.

6.1 Thermodynamics experiments

An electric thermometer is used to obtain the accurate surface temperature of the SMA plates. The probe (diameter: 3 mm) of the thermometer is embedded between SMA plate and copper wire, and feedbacks the temperature to the computer when the SMA plate is actuated. Fig. 14 shows the experimental results of the actuation speed with respect to various currents.

The curves in Fig. 14 are similar to that of simulation results in Fig. 12. The curves can be classified into two categories, which is in accordance with the thermal simulations. In the cases with the currents of 0.8 A, 1 A, and 1.5 A the temperature can not reach A_f, because of the low heat flux. The equivalent convective heat transfer coefficient h_w is measured as 2250 $w \cdot m^{-2} \cdot K^{-1}$. As for the cases with the currents ranging from 2 A to 4.5 A, the actuation time for temperature reaching A_f becomes shorter with the increase in the current. The minimum heating time occurs with the current of 4.5 A, which is only 0.35 s. For each curve of the currents (from 2 A to 4.5 A), the changing rate of the temperature declines within the interval [46˚C, 54˚C], which corresponds exactly to the thermal simulations. However, if the current is the same, the actuation speed in simulation is all higher than that in experiments. Furthermore, when I equals to 1.5A, it can't reach A_f in the experiment which is different from the simulation result. The reason is that the real h_w is higher than that of the simulation and the three assumptions are set which neglect some energy such as heat radiation. The cooling time is about 0.95 s for all the cases with the currents changing form 2 A to 4.5 A, which is in accordance with the simulation results.

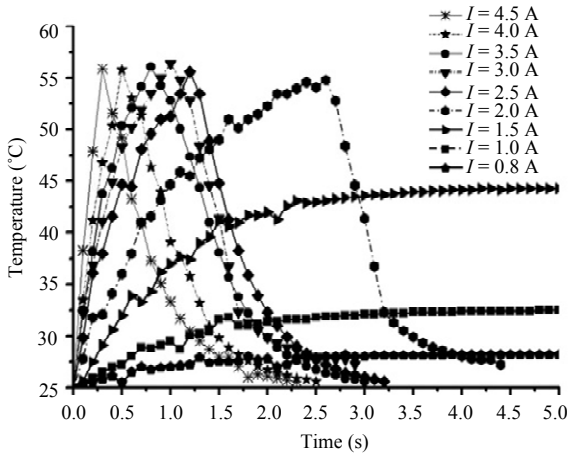

Fig. 14 Temperature of the SMA plate underwater with respect to various currents. In the cases with the currents of 0.8 A, 1 A and 1.5 A, the balance temperature are 28.2˚C, 32.5˚C and 44.3˚C respectively, and in the cases with the currents of 2 A, 2.5 A, 3 A , 3.5 A, 4 A and 4.5 A, the actuation time are 2.5 s, 1.2 s, 1 s, 0.81 s, 0.45 s and 0.35 s, respectively.

6.2 Angular displacement in actuation experiments

The angular displacement of the SMA plate is so important as to directly affect the motion range of the SMA pectoral fin. Fig. 15 shows angular displacement changing with time with respect to various currents. The curves can also be classified into two categories. When the current is not high enough to increase the temperature up to the transformation temperature (I = 0.8 A, 1 A and 1.5 A), the SMA plate keeps still or bends slightly. As the current rises, the angular displacement of the SMA plate can reach the maximum angle of 121˚. The angular displacement increases rapidly during the transformation and keeps stable afterwards.

Comparing the simulation results, we can conclude that the curves share the same shapes and trends. However, the response time in the experiments is longer than that in the simulations. Besides, when I equals to 1.5 A, it can reach the largest angular displacement in the simulation, but it's not the case with the experiment. The possible reason is that the three assumptions in the thermodynamics simulations and neglected energy dissipation.

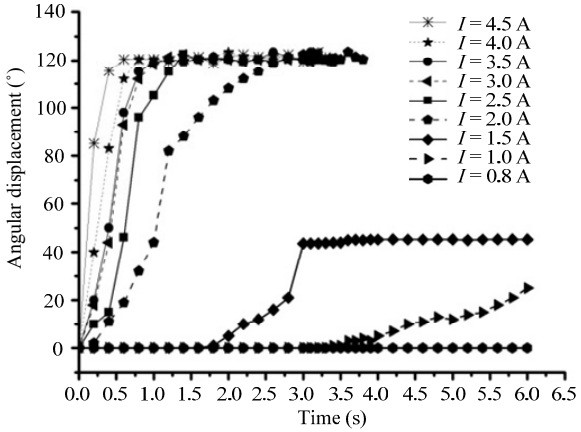

Fig. 15 Angular displacement of the SMA plate underwater with respect to various currents. h_w equals to 2250 $w \cdot m^{-2} \cdot K^{-1}$.

6.3 The influence of the thickness of SMA plates

The influence of the thickness of SMA plates on output torque is also investigated by experiments. The results are shown in Fig. 16. The torque increases with the thickness of the SMA plate. When the thickness is 2.5 mm, the torque output can reach a substantial value, i.e. 910 N·mm.

The energy for phase transformation increases with the plates thickness, which leads to a lower actuation speed. According to the output torque illustrated in Fig. 16, there is an optimal thickness to obtain an enough torque with a relative high actuation speed. Based on the experimental results, SMA plate with the thickness of 1 mm is a good choice because it can actuate fast and output a relative large torque simultaneously.

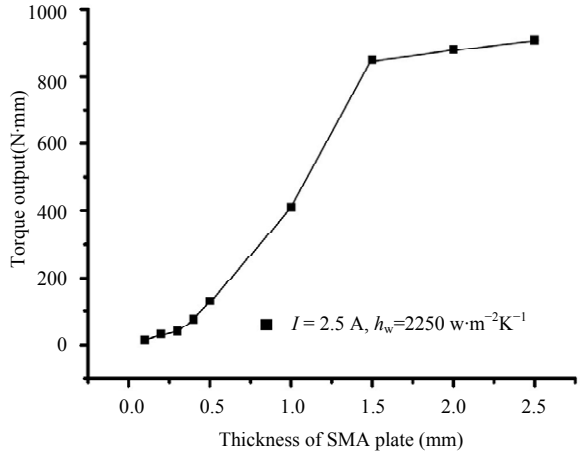

Fig. 16 Relationship between the torque output and the thickness of SMA plates.

7 Conclusions and future work

A novel mechanical design of a flexible pectoral fin based on SMA capable of performing 3D motions has been presented in this paper. First we conducted a morphological study on the pectoral fins of a carp, and obtained the distribution of the bending stiffness and Young's modulus of the fin ray. Then we developed a robotic pectoral fin prototype, and conducted a series of simulations and experiments to investigate the performance of the SMA fin ray. The following results were obtained: (1) the speed of temperature change of the SMA plate increases with the applied current; (2) the actuation speed of angular displacement increases with the current; and (3) the torque output increases with the thickness of the SMA plate. The experimental results correspond to those obtained in the simulations, which lay a good basis for the control of the robotic pectoral fin.

In the future work, the following efforts are helpful to enhance the 3D robotic fin: (1) more SMA fin ray controlling experiments; (2) a series of experiments to investigate the thrust, lift force and span-wise force produced by the robotic pectoral fin under different gestures; and (3) installing the robotic pectoral fins to the previously developed robotic fish[19], and observing the influence of the pectoral fins on the balance and the maneuver of the robotic fish. As for multi-actuated fin rays with a number of control variables, it might be useful to consider ANOVA[28] and control scheme with Central Pattern Generator (CPG)[29,30] in the future study.

Acknowledgments

This research has been financially supported by National Natural Science Foundation of China (50975270) and the Fundamental Research Funds for the Central Universities (WK2090090002). The authors thank Ms. Qiang Yun sincerely for her helpful revision and polishing to the manuscript.

References

[1] Webb P W. Form and function in fish swimming. *Scientific American*, 1984, **25**, 58–68.

[2] Lauder G V, Madden P, Hunter I. Design and performance of a fish fin-like propulsor for AUVs. *Proceedings of* 14*th International Symposium on Unmanned Untethered Submersible Technology*, Durham, New Hampshire, USA, 2005.

[3] Epstein M, Colgate J, Maciver M. Generating thrust with a biologically-inspired robotic ribbon fin. *Proceedings of the IEEE International Conference on Intelligent Robots and Systems*, Beijing, China, 2006, 2412–2417.

[4] Triantafyllou M S, Triantafyllou G S. An efficient swimming machine. *Scientific American*, 1995, **272**, 64–70.

[5] Yu J Z, Wang L. Parameter optimization of simplified propulsive model for biomimetic robot fish. *Proceedings of the IEEE International Conference on Robotics and Automation*, Barcelona, Spain, 2006, 3306–3311.

[6] Liu J, Hu H. Biological inspiration: from carangiform fish to multi-joint robotic fish. *Journal of Bionic Engineering*, 2010, **7**, 35–48.

[7] Lauder G V, Peter G, Madden A. Fish locomotion: kinematics and hydrodynamics of flexible foil-like fins. *Experiments in Fluids*, 2007, **43**, 641–653.

[8] Lauder G V. How fishes swim: flexible fin thrusters as an EAP platform. *Proceedings of the International Society for Optics and Photonics*, San Diego, California, USA, 2007, **6524**, 652402.

[9] Lauder G V, Liem K F. The evolution and interrelationships of the actinopterygian fish. *Bulletin of the Museum of Comparative Zoology*, 1983, **150**, 95–197.

[10] Tytell E, Standen E, Lauder G. Escaping flatland: three-dimensional kinematics and hydrodynamics of median fins in fishes. *The Journal of Experiments Biology*, 2008, **211**, 187–195.

[11] Low K H, Yang J, Pattathil A P, Zhang Y H. Initial prototype design and investigation of an undulating body by SMA. *Proceedings of the IEEE International Conference on Automation Science and Engineering*, Shanghai, China, 2006, 472–477.

[12] Low K H. Mechatronics and buoyancy implementation of robotic fish with modular fin mechanisms. *Proceedings of the Institution of Mechanical Engineers*, *Part I*: *Journal of Systems and Control Engineering*, 2007, **221**, 295–309.

[13] Low K H. Modelling and parametric study of modular undulating fin rays for fish robots. *Mechanism and Machine Theory*, 2009, **44**, 615–632.

[14] Toda Y, Suzuki T, Uto S, Tanaka N. Fundamental study on a fish-like body with two undulating side fins. In: Kato N, Kamimura S (Eds.), *Bio-mechanisms of Swimming and Flying*, Springer, Berlin, Germany, 2004, 93–110.

[15] Toda Y, Ikeda H, Sogihara N. The motion of a fish-like under-water vehicle with two undulating side fins. *Proceedings of the* 3*rd International Symposium on Aero Aqua Bio-mechanisms*, Okinawa, Japan, 2006.

[16] Hu T, Shen L, Lin L, Xu H. Biological inspirations, kinematics modeling, mechanism design and experiments on an undulating robotic fin inspired by Gymnarchus niloticus. *Mechanism and Machine Theory*, 2009, **44**, 633–645.

[17] Wang Z, Wang Y, Li J, Hang G. A micro biomimetic manta ray robot fish actuated by SMA. *Proceedings of the IEEE International Conference on Robotics and Biomimetics*, GuiLin, China, 2009.

[18] Wang Z, Hang G, Wang Y, Li J, Du W. Embedded SMA wire actuated biomimetic fin: a module for biomimetic underwater propulsion. *Smart Materials and Structures*, 2008, **17**, 025039.

[19] Yan Q, Han Z, Zhang S, Yang J. Parametric research of experiments on a Carangiform robotic fish. *Journal of Bionic Engineering*, 2008, **5**, 95–101.

[20] Zhang Y, He J, Yand J, Zhang S, Low K. A computational fluid dynamics (CFD) analysis of an undulatory mechanical fin driven by shape memory alloy. *International Journal of Automation and Computing*, 2006, **4**, 374–381.

[21] Zhang Y, He J, Yand J, Zhang S, Low K. Design and investigation of shape memory alloy driven flexible pectoral fin. *Proceedings of IEEE International Conference on Robotics and Biomimetics*, Kunming, China, 2006.

[22] Lauder G, Madden P, Mittal R, Dong H, Bozkurttas M. Locomotion with flexible propulsors: I. Experimental analysis of pectoral fin swimming in sunfish. *Bionispiration & Biomimetics*, 2006, **1**, S25–S34.

[23] Mittal R, Dong H, Bozkurttas M, Lauder G V, Madden P. Locomotion with flexible propulsors: II. Computational modeling of pectoral fin swimming in sunfish. *Bionispiration & Biomimetics*, 2006, **1**, S35–S41.

[24] Tanaka K. A thermomechanical sketch of shape memory effect: one-dimensional tensile behavior. *Res Mechanica*, 1986, 251–263.

[25] Liang C, Rogers C A. One-dimensional thermomechanical constitutive relations for shape memory material. *Journal of Intelligent Material Systems and Structures*, 1990, **1**, 207–234.

[26] Brison L C. One-dimensional constitutive behavior of shape memory alloys: thermomechanical derivation with non-constant material functions. *Journal of Intelligent Material Systems and Structures*, 1993, 4, 229–242.

[27] Yang K, Gu C L. Modelling, simulation and experiments of novel planar bending embeded SMA actuators. *Mechatronics*, 2008, **18**, 323–329.

[28] Low K H, Chong C W. Parametric study of the swimming performance of a fish robot propelled by a flexible caudal fin. *Bioinspiration & Biomimetics*, 2010, **5**, 046002**.**

[29] Ijspeert A J, Crespi A, Ryczko D, Cabelguen J M. From swimming to walking with a salamander robot driven by a spinal cord model. *Science*, 2007, **315**, 1416–1420.

[30] Zhou C, Low K H. Posture analysis and experiments of bionic fish propelled by paired pectoral foils. *ASME Transactions on Mechatronics*, 2012, in Press.